Probabilistic Engineering Mechanics 59 (2020) 103046

Contents lists available at ScienceDirect

Probabilistic Engineering Mechanics

journal homepage: www.elsevier.com/locate/probengmech

Probabilistic modeling and simulation of wave speeds in random composites

Sarah C. Baxter *, Katherine A. Acton

Department of Mechanical Engineering, University of St. Thomas, St. Paul MN, 55105, United States of America

ARTICLE INFO

Keywords:
Probabilistic methods
Statistical volume elements
Random composites
Mesoscale micromechanics

ABSTRACT

Investigations of wave propagation in composite materials have been used both to experimentally measure material properties and to validate material property model characterizations. For continuous fiber reinforced composites, these characterizations often have relied on a bulk description of the effective behavior of a Representative Volume Element (RVE) and assumed ideal conditions of transverse isotropy and a well defined direction of the fibers. Analytic models, based on these composite properties and fiber directions, can then be used to predict the speeds of waves propagating through the material. The goal of this work is to develop a probabilistic simulation to examine how variations in the composite properties and small angles of misalignment of the fibers affect wave speed. To achieve this, a joint probability function is constructed where a dominant material property and the angle of fiber orientation are considered independent random variables. Sampling from this joint distribution produces pairs of parameters that can be input into wave speed analysis. The resulting wave speed distributions can be used to characterize the joint effects of randomness in material property and fiber angle.

1. Introduction

Probabilistic modeling of the random properties of composite materials has the potential to provide more realistic estimates of the mechanical behavior of these materials and to help understand the elements of material design. Capturing variability of a property, however, is only the first step. The next is to be able to simulate a response based on that variable or random description. In many cases, this will involve including more than one random variable into a simulation process. This work illustrates the process whereby wave speeds in a random fiber reinforced composite material can be modeled and simulated. Wave speed is cast as a function of two random variables, depending on both a primary, with respect to wave speed, material property and the angle of fiber orientation relative to the direction of wave propagation. A joint probability distribution function is constructed and parameters pairs sampled from this distribution and used to simulate wave speeds.

Wave propagation has a long history related to composite material modeling. Low frequency waves have been used both to experimentally identify material properties [1,2] as well as validate mechanical models [3]. Much of the literature devoted to wave propagation in transversely isotropic media relates to geophysical applications, where wave propagation measurements are used to estimate properties of layered rock [4,5]. A comprehensive study of wave propagation in anisotropic media can be found in [6].

It has been shown in [1,6], among others, that solution of the Kelvin–Christoffel equation [7], leads to a determination of wave phase velocities. These velocities are given as a function of material properties and the incident angle of wave propagation through a transversely isotropic medium. Equations adapted from this analysis are presented in what follows. Consider a transversely isotropic fiber reinforced composite with the fiber direction labeled x_3 and the $x_1 - x_2$ plane designated as the transverse plane of isotropy. Such a cross-section is shown in Fig. 1. If v is the wave velocity, ρ is the density, and θ is the angle between the preferred or fiber direction and the direction of propagation of the wave, then the velocity of a transverse wave is given by

$$v = [(C_{66}\cos^2\theta + C_{44}\sin^2\theta)/\rho]^{1/2}. \tag{1}$$

The C_{ij} terms are elements of the stiffness tensor, **C** of the composite. Eq. (1) models transverse waves that have displacements perpendicular to the plane which contains the preferred direction (fiber) and the propagating direction of the wave. This formula reduces to velocities in the fiber direction and perpendicular to the fiber direction when $\theta = 0°$ or 90°, respectively.

Waves that are not purely transverse or purely longitudinal (displacements in the propagating direction) have wave speeds represented by the following quadratic equation in v^2

$$(C_{33}\cos^2\theta + C_{66}\sin^2\theta - \rho v^2)(C_{11}\sin^2\theta + C_{66}\cos^2\theta - \rho v^2) = (C_{66} + C_{23})^2\cos^2\theta\sin^2\theta. \tag{2}$$

* Corresponding author.
E-mail address: scbaxter@stthomas.edu (S.C. Baxter).

https://doi.org/10.1016/j.probengmech.2020.103046
Received 16 January 2020; Accepted 31 January 2020
Available online 5 February 2020

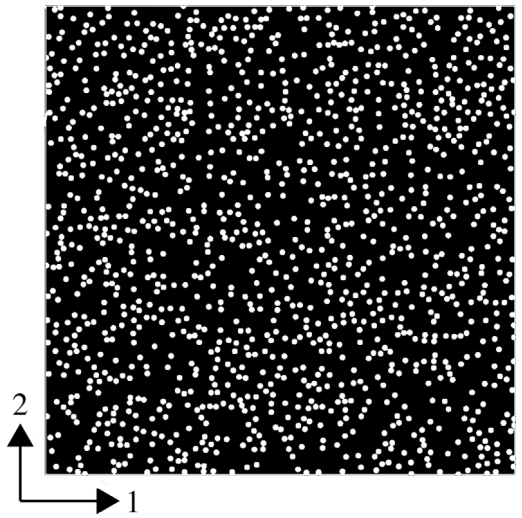

Fig. 1. Representative Volume Element (RVE) of the transverse section of a composite microstructure with uniformly randomly distributed fibers; fibers have circular cross sections.

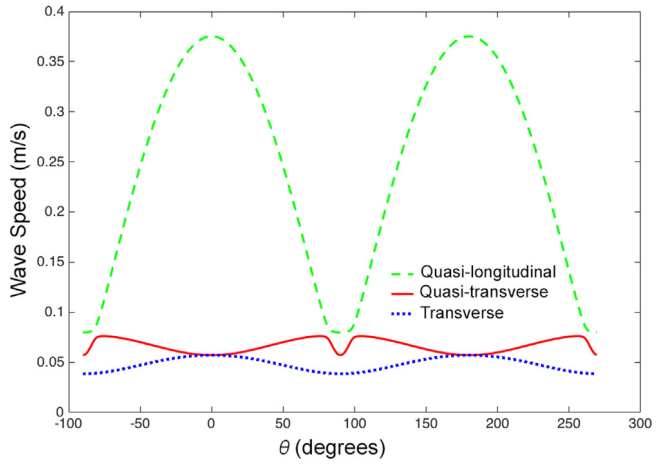

Fig. 2. Plots of wave speeds for transverse, quasi-transverse and quasi-longitudinal, from Eqs. (1), (2), for a fixed set of stiffnesses over a wide range of θ.

The resulting waves are referred to as quasi-longitudinal, quasi-transverse waves. Fig. 2 shows plots of Eq. (1) and the real, positive and negative roots of Eq. (2) over a wide range of θ. In what follows, a narrower range of θ is considered.

Material properties in composites are often described as isotropic or transversely isotropic in a bulk, or effective sense, at the scale of a Representative Volume Element (RVE). This characterization is accurate where the scale of variation of the material morphology is much less than the scale of the macroscopic deformation. In the study of wave propagation, an effective medium is termed "long wave equivalent" where it behaves as a homogeneous medium for wave lengths larger than a given characteristic length [8].

Accurate RVE characterization is the focus of much study [9]. Clearly, this characterization is centrally important to the validity of any analysis that results from it. Statistical Volume Elements (SVE) are partitions of an RVE into smaller elements. Unlike the effective properties derived from an RVE, homogenization of SVEs results in apparent properties; these are not unique because they depend on boundary conditions. To assess the convergence of material properties with increasing volume element size, a hierarchy of bounds on SVE has been developed [10–12]. This hierarchy of bounds is briefly stated here, for further details, see also [13]:

$$[C_R] \equiv \langle S_1^S \rangle^{-1} \leq \langle S_{\delta'}^S \rangle^{-1} \leq \langle S_{\delta}^S \rangle^{-1} \leq [C^{eff}] \leq \langle C_{\delta}^K \rangle \leq \langle C_{\delta'}^K \rangle \leq \langle C_1^K \rangle \equiv [C_V] \quad \forall \delta > \delta' \tag{3}$$

where $[C^{eff}]$ is the effective constitutive tensor, $[C_R]$ and $[C_V]$ are the Reuss and Voigt bounds, respectively, $[C^K]$ is the apparent stiffness tensor obtained from a kinematically uniform boundary condition test of the material, $[S^S]$ is the apparent compliance obtained from a statically uniform boundary condition test of the material, δ, δ' are characteristic sizes of the SVE, and $\langle \cdot \rangle$ denotes volumetric averaging.

The statistics of the population of SVE properties can provide a consistent and repeatable method to approximate the variability of properties due to the random microstructure [10,14–17]. In this work, a population of SVE will be used to generate a probability distribution whose mean value is an upper bound on the effective behavior of the RVE and characterizes local variability. Here, this variability is used to approximate variability in effective material properties.

An additional layer of complexity occurs when a wave is propagating through a material with inherently random microstructural characteristics and the angle between the wave propagating direction and the orientation of fibers is uncertain. This angle of orientation may be variable due to experimental error, or localized mis-alignment of the fibers from the manufacturing process. The alignment error may be considered small, yet results may be substantially affected, especially where there is a high degree of anisotropy. Here, angular orientation will be modeled with a Gaussian distribution for a small range of angles as might be expected from experimental error or inexact manufacturing.

For a transversely isotropic material, such as that studied in this work, it is possible to identify a single property on which all of the other properties needed for modeling are conditionally dependent. Developing approximations of this conditional dependence allows wave speed to be modeled using single random material property. Fiber orientation, or mis-alignment, is independent of material properties. As a result wave speed can be cast as a two dimensional random variable, a function of a single material property and angular orientation, $v(C_{ij}, \theta)$, based on Eqs. (1), and (2).

It is from this perspective that the wave speeds in a transversely isotropic composites are studied. A joint distribution function of the two random variables is constructed. Subsequent sampling from this distribution produces a distribution of parameter pairs that are used to simulate a population of wave speeds. Unlike an RVE-based calculation, this population of wave speeds will contain variability characteristic of a material whose effective properties include fluctuations. Conclusions are then drawn about the relative significance of uncertainty due to material properties, and uncertainty in wave angle relative to fiber direction.

2. Construction of Statistical Volume Elements (SVE)

This work extends the results of previous work, which focused on determining distributions of random properties based on a meso-scale mechanical analysis of Statistical Volume Elements (SVE) [14]. In this work, as in [14], the material RVE is as shown in Fig. 1. This RVE represents a transverse section of the composite with uniformly distributed circularly cross-sectioned fibers. The centers of the fibers are distributed randomly according to a Poisson process. The composite phases, fiber and matrix, are assumed isotropic. The fiber was assigned an elastic modulus of 100 GPa and the matrix an elastic modulus of 1 GPa; for simplicity in modeling, both phases were assigned a Poisson's ratio of $\nu = 0.3$. The fiber volume fraction is approximately 12%. Based on its construction, the composite is assumed to be statistically isotropic in the plane of the RVE. Properties based on a finite element analysis suggest that this is a reasonable assumption.

To construct the SVEs, the RVE was first divided into cells using Voronoi tessellation. The Voronoi cells were constructed using each

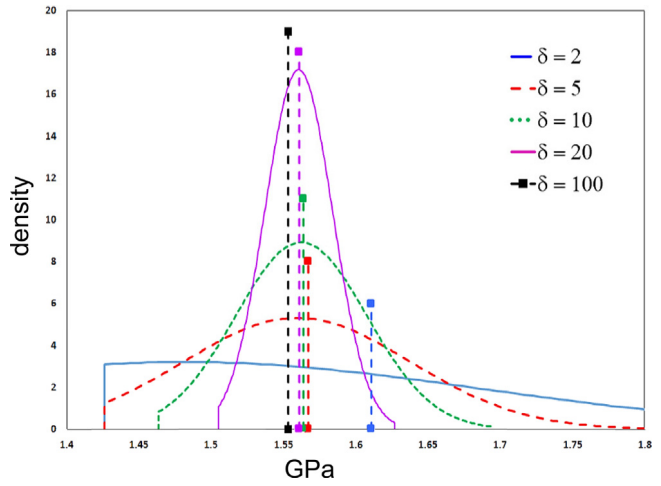

Fig. 3. Probability distribution functions based on SVE sizes $\delta = 2, 5, 10$, and 20 for RVE size $\delta = 100$ (shown in Fig. 1), with material contrast ratio 100 : 1 [14].

fiber cross-section as a center point. The cell then contains all points that lie closer to one single fiber than to any other. Using this approach, with a relatively small fiber radius, Voronoi cell boundaries do not intersect any of the inclusions. Preventing the stiff fibers from intersecting the SVE partition boundaries has been shown to reduce the impact of contrast ratio on property bounds, make the choice of partition size less critical to a mesoscale model and results in a model that is better able distinguish between subtle microstructural differences [14].

Next, a square grid was laid over the tessellated RVE and SVEs were assembled by grouping together all of the cells whose centroids were within an individual square grid. The partition size was then defined as the size of the square grid [14]. This work will focus on one partition size, $\delta = 10$, where δ is defined as $\delta = l_{SVE}/d$; d is the inclusion diameter, and l_{SVE} is the length of a single square in the overlaid grid. Because only 100 SVEs result from a partition using $\delta = 10$ partition size, data from a second microstructure, generated using the same process, was included in the analysis.

In order to calculate apparent properties of each SVE, a set of uniform displacement, plane strain boundary value problems were solved using a finite element analysis. Uniform displacement boundary conditions are more appropriate for implementation in FEA, which enforces continuity of displacements but not necessarily continuity of tractions. Properties were then calculated from the strain energy U given by [10]:

$$\begin{aligned} U &= \frac{V}{2}\{\bar{\sigma}_{ij}\epsilon^0_{ij}\} \\ &= \frac{V}{2}\epsilon^0_{ij}C_{ijkl}\epsilon^0_{ij} \\ &= \frac{V}{2}[C_{1111}(\epsilon^0_{11})^2 + C_{2222}(\epsilon^0_{22})^2 + C_{1212}(\epsilon^0_{12})^2 \\ &\quad + 2\epsilon^0_{11}C_{1122}\epsilon^0_{22} + 2\epsilon^0_{22}C_{2212}\epsilon^0_{12} + 2\epsilon^0_{12}C_{1211}\epsilon^0_{11}]. \end{aligned} \tag{4}$$

V is the material volume, $\bar{\sigma}_{ij}$ is the volume average of stress, ϵ^0_{ij} is the constant loading strain and the C_{ijkl} are elements of the constitutive stiffness tensor. These apparent properties correspond to upper bounds on the effective properties.

Fig. 3 [14] shows distributions of the apparent property C_{1111}, as calculated from Eq. (4). This result is an element of the tensor $[C^K_\delta]$ in Eq. (3), where $\delta = 2, 5, 10$ and 20. As expected given the hierarchy of bounds, the mean of each set of SVE approaches the RVE effective property with increasing SVE size. The standard deviation decreases with increasing SVE size. In this work, as in the previous work, probability distribution functions (PDF) are constructed using the Principle of Maximum Entropy (PME).

Table 1
Statistical comparison of in-plane normal SVE apparent properties; C_{11} vs C_{22}. Here ρ is the Pearson correlation coefficient between the two stiffnesses.

	Mean (GPa)	Var	Skew	ρ
C_{11}	1.18598	0.00136	0.347	–
C_{22}	1.18612	0.00133	0.388	0.962

Table 2
Statistical comparison of in-plane normal vs. shear SVE apparent properties; C_{11} vs C_{66}. ρ is the Pearson correlation coefficient between the two stiffnesses.

	Mean (GPa)	Var	Skew	ρ
C_{11}	1.18598	0.00136	0.347	–
C_{66}	0.5752	0.00020	0.3824	0.9828

3. Transversely isotropic SVE model

Based on the approach described above, components of the elastic stiffness tensor, $C_{1111} = C_{11}$, $C_{2222} = C_{22}$ and $C_{1212} = C_{66}$, were approximated for each SVE. These can be obtained from the strain energy using simple loading conditions. They represent properties in the transverse $(x_1 - x_2)$ plane of the fiber-reinforced composite.

A statistical analysis was performed on this data. Results comparing the two in-plane normal stiffnesses are shown in Table 1, and indicate that the in-plane normal stiffnesses, C_{11} and C_{22}, are highly correlated and have similar means, variance and skew. Marginal distributions of the SVE properties were constructed using PME as in [14]. These univariate PDFs are compared in Fig. 4a. A plot of C_{11} vs C_{22} is shown in Fig. 4b. In prior work, [14], several partition sizes were considered. As the partition size decreased, individual SVEs could no longer be approximated as isotropic. However, for the partition size of $\delta = 10$, these results suggest that the assumption of isotropy for individual SVEs is a reasonable one.

Comparisons of the in-plane normal stiffness and the in-plane shear stiffness, C_{11} and C_{66}, are shown in Table 2. These properties are also highly correlated but have significantly different means and an order of magnitude difference in the variance. Fig. 4c shows the two marginal distributions for C_{11} and C_{66}. These comparisons suggest that the in-plane normal stiffness C_{11} and the in-plane shear stiffness C_{66} are conditionally dependent.

The wave speed model given by Eq. (1) requires C_{44} and C_{66}. The model given by Eq. (2) requires C_{11}, C_{33}, C_{66} and $C_{23} = C_{13}$. By taking advantage of the assumption of transverse isotropy and approximating the conditional dependence between parameters it is possible to present the wave speeds as functions of a single material property, C_{66}.

A linear regression line was fit to fiber volume fraction, vf, and C_{66}; these data sets were drawn from the SVE analysis. This regression function line was an excellent fit to the data. These linear functions will be used to approximate vf from a simulated value of C_{66}. A linear regression line was fit to C_{11} and C_{66}, which was also an excellent fit. The longitudinal modulus E_3 and the major Poisson's ratio (longitudinal-transverse), ν_{31} were approximated by a rule of mixtures using the vf was approximated above as a function of C_{66}.

For materials with a high contrast ratio, i.e. fibers much stiffer than the matrix, the longitudinal-transverse shear modulus can be modeled [18], as

$$G_{13} = \frac{G_m}{1 - vf} = \frac{1}{C_{44}}, \tag{5}$$

where G_m is the shear modulus of the matrix. In this way C_{44} can be approximated using the vf approximated above as a linear function of C_{66}. Wave speeds defined in Eq. (1) are then simulated by sampling values of C_{66} (and θ) and approximating C_{44}.

For a transversely isotropic material, with the fiber direction x_3 and transverse plane $x_1 - x_2$, the stress–strain relationship for a transversely

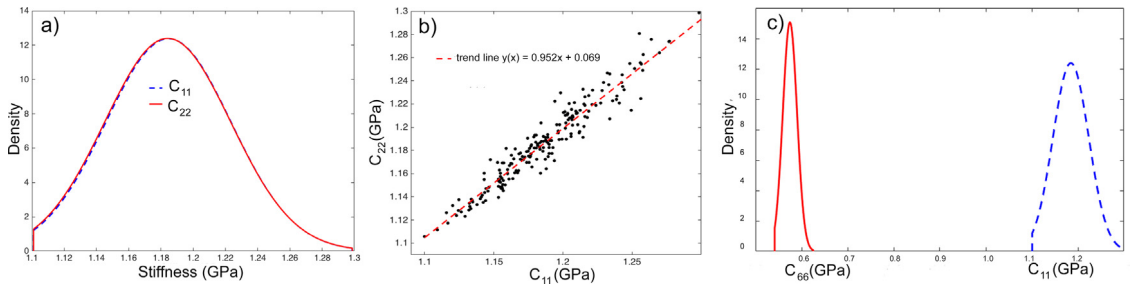

Fig. 4. Plot showing, (a) the overlapping distribution functions for C_{11} and C_{22} (b) paired values of C_{11} vs C_{22}, $C_{11} \approx C_{22}$ and (c) in-plane normal and shear stiffness C_{11} and C_{66}, show distinct marginal distributions.

isotropic material is given in terms of the stiffness tensor by

$$\boldsymbol{\sigma} = \boldsymbol{C}\boldsymbol{\epsilon}. \tag{6}$$

The compliance tensor, $\mathbf{S} = \mathbf{C}^{-1}$ is given by

$$\begin{bmatrix} \epsilon_1 \\ \epsilon_2 \\ \epsilon_2 \\ \gamma_{23} \\ \gamma_{13} \\ \gamma_{12} \end{bmatrix} = \frac{1}{\Delta} \begin{bmatrix} C_{11}C_{33} - C_{13}^2 & C_{13}^2 - C_{12}C_{33} & (C_{12} - C_{11})C_{13} & 0 & 0 & 0 \\ C_{13}^2 - C_{12}C_{33} & C_{11}C_{33} - C_{13}^2 & (C_{12} - C_{11})C_{13} & 0 & 0 & 0 \\ (C_{12} - C_{11})C_{13} & (C_{12} - C_{11})C_{13} & C_{11}^2 - C_{12}^2 & 0 & 0 & 0 \\ 0 & 0 & 0 & \frac{\Delta}{C_{44}} & 0 & 0 \\ 0 & 0 & 0 & 0 & \frac{\Delta}{C_{55}} & 0 \\ 0 & 0 & 0 & 0 & 0 & \frac{\Delta}{C_{66}} \end{bmatrix} \times \begin{bmatrix} \sigma_1 \\ \sigma_2 \\ \sigma_3 \\ \tau_{23} \\ \tau_{13} \\ \tau_{12} \end{bmatrix} \tag{7}$$

where $\Delta = (C_{11} - C_{12})[(C_{11} + C_{12})C_{33} - 2C_{12}^2]$, and $S_{33} = 1/E_3$.

In terms of the engineering constants, $\mathbf{S}$ is given by

$$\begin{bmatrix} \epsilon_1 \\ \epsilon_2 \\ \epsilon_2 \\ \gamma_{23} \\ \gamma_{13} \\ \gamma_{12} \end{bmatrix} = \frac{1}{\Delta} \begin{bmatrix} \frac{1}{E_1} & \frac{-\nu_{21}}{E_2} & \frac{-\nu_{31}}{E_3} & 0 & 0 & 0 \\ \frac{-\nu_{12}}{E_1} & \frac{1}{E_1} & \frac{-\nu_{32}}{E_3} & 0 & 0 & 0 \\ \frac{-\nu_{13}}{E_1} & \frac{-\nu_{23}}{E_2} & \frac{1}{E_3} & 0 & 0 & 0 \\ 0 & 0 & 0 & \frac{\Delta}{G_{23}} & 0 & 0 \\ 0 & 0 & 0 & 0 & \frac{\Delta}{G_{13}} & 0 \\ 0 & 0 & 0 & 0 & 0 & \frac{\Delta}{C_{12}} \end{bmatrix} \begin{bmatrix} \sigma_1 \\ \sigma_2 \\ \sigma_3 \\ \tau_{23} \\ \tau_{13} \\ \tau_{12} \end{bmatrix} \tag{8}$$

Using the rule of mixtures approximations of E_3, from Eqs. (7) and (8),

$$E_3 = C_{33} - \frac{C_{13}^2}{C_{11} - C_{66}}. \tag{9}$$

Substituting this into

$$\frac{-\nu_{31}}{E_3} = \frac{C_{31}}{-2C_{13}^2 + C_{11}C_{33} + C_{12}C_{33}}, \tag{10}$$

and simplifying, yields

$$C_{23} = C_{13} = \frac{\nu_{31}}{C_{11} - C_{66}}. \tag{11}$$

Density was assumed to be constant and calculated using a rule of mixtures and assuming a fiber volume fraction of 0.12. Density of the fiber and matrix were approximated with those of a high modulus carbon fiber and an epoxy matrix; a composite made of these materials has a contrast ratio of ≈343/3.5 = 98, similar to the model material studied here.

4. Joint probability distributions

For many simulations modeling is done by sampling from a distribution. In previous work [14], marginal (univariate) distributions were developed using the Principle of Maximum Entropy (PME) to compare and contrast the effect of partition size, contrast ratio, and microstructure on the distribution of composite properties. While the underlying assumptions of the boundary conditions used in creating the SVEs and the constraints adopted using PME do not represent the exact random field of an apparent property [19], these marginal distributions were shown to be a way to visually distinguish the differences between the effects of microstructure and partitioning size. The procedure for developing these marginal distributions can be found in [14,20].

However, in many cases predictive models of mechanical behavior may involve a bivariate or joint distributions, where each of two random variables falls in a range that is specific to each individual variable. One such case is the determination of the velocities of ultrasonic waves propagating in various directions through the composite. This is the case for the wave speeds described above. A bivariate form of the PME, therefore, was used to construct a joint distribution function between the elastic stiffness C_{66} of a composite and the angular orientation of the fibers, from $\theta = \pm 25°$. Thus wave speed $v(C_{66}, \theta)$ is approximated as a two-dimensional random variable.

The Principle of Maximum Entropy (PME) is based on the idea that the 'best' probability density function describing a dataset is the one that maximizes the uncertainty, provided that one accounts for all *a prioi* information. This optimization results in a solution with the maximum uncertainty, or the minimum embedded bias [21]. PME has previously been used in combination with random matrix theory to characterize the convergence of effective properties with increasing size of mesoscale volume elements [22]. It has also been used in the reconstruction of material microstructures [23] to model the evolving properties of percolating nanostructures [24] and shown to be an effective method of developing prior probability distributions for Bayesian inference [25].

A PME based joint probability distribution function $p(x, y)$, is the function that maximizes Shannon's entropy functional, H, [21] given

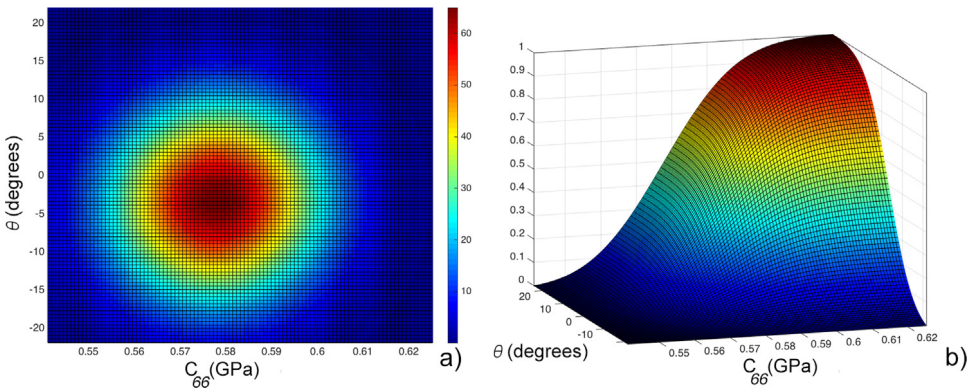

Fig. 5. Joint PME-PDF of C_{66} and θ. (a) 2D rendering of joint PDF (b) cumulative distribution. As defined by the PME, density is zero outside the range of the stiffnesses defined by the SVE. The values of θ are defined by a continuous normal distribution.

by

$$H[p(x,y)] = -\int_{-\infty}^{\infty} p(x,y)\ln[p(x,y)]\,dx\,dy. \tag{12}$$

Maximizing this functional results in the general form of a two dimensional PME-PDF

$$p(x,y) = f(x,y) = \lambda_0 + \lambda_1 x + \lambda_2 y + \lambda_3 xy + \lambda_4 x^2 + \lambda_5 y^2, \tag{13}$$

where the λ_i, are Lagrange multipliers chosen to satisfy constraints associated with a distribution function. In particular, the statistical moments of the PME-PDF must match those of the data as well as the standard normalization of a density function, i.e. the integral of the PDF must be one. Additionally, since the population of apparent properties are bounded, with minimums, x^-, y^- and maximums, x^+, y^+, the PDF is assumed to be zero outside of these ranges.

The generalization of statistical moments for multivariate distributions is fairly straightforward [26]. A bivariate joint distribution function $p(x,y)$ will have a central moments of order k,l defined as

$$\mu_{kl} \equiv \mathcal{E}\left[(x-\mu_x)^k (y-\mu_y)^l\right] = \int\int (x-\mu_x)^k (y-\mu_y)^l p(x,y)dx\,dy \tag{14}$$

where $\mathcal{E}$ is the expected value and μ_x, μ_y are the mean values of x and y respectively. The function must satisfy the following conditions

$$\int_{Y_{min}}^{Y_{max}}\int_{X_{min}}^{X_{max}} p(x,y)\,dx\,dy = 1 \quad \text{(0th normalization)}, \tag{15}$$

$$\int_{Y_{min}}^{Y_{max}}\int_{X_{min}}^{X_{max}} (x-\mu_x)p(x,y)\,dx\,dy = \mu_{10} \tag{16}$$

$$\int_{Y_{min}}^{Y_{max}}\int_{X_{min}}^{X_{max}} (y-\mu_y)p(x,y)\,dx\,dy = \mu_{01} \tag{17}$$

$$\int_{Y_{min}}^{Y_{max}}\int_{X_{min}}^{X_{max}} (x-\mu_x)(y-\mu_y)p(x,y)\,dx\,dy = \mu_{11} \text{ (covariance)}, \tag{18}$$

$$\int_{Y_{min}}^{Y_{max}}\int_{X_{min}}^{X_{max}} (y-\mu_y)^2 p(x,y)\,dx\,dy = \mu_{02} \tag{19}$$

$$\int_{Y_{min}}^{Y_{max}}\int_{X_{min}}^{X_{max}} (x-\mu_x)^2 p(x,y)\,dx\,dy = \mu_{20} \tag{20}$$

Discrete forms of these multivariate moments can be approximated from the data using

$$\mu_{10} = \frac{1}{N}\sum_{i=1}^{N}(x_i - \mu_x) \tag{21}$$

$$\mu_{01} = \frac{1}{N}\sum_{i=1}^{N}(y_i - \mu_y) \tag{22}$$

$$\mu_{11} = \frac{1}{N}\sum_{i=1}^{N}(x_i - \mu_x)(y_i - \mu_y) \tag{23}$$

$$\mu_{02} = \frac{1}{N}\sum_{i=1}^{N}(y_i - \mu_y)^2 \tag{24}$$

$$\mu_{20} = \frac{1}{N}\sum_{i=1}^{N}(x_i - \mu_x)^2 \tag{25}$$

Here, μ_r is used to denote the sample rather than the population mean.

5. Results

The univariate probability distribution of C_{66} was developed from SVE data. The distribution of θ was assumed Gaussian with a mean of zero and standard deviation of 0.15, which resulted in an approximate range of $\theta \in [-25°, 25°]$. Paired data parameters, (C_{66}, θ) were sampled from the joint distribution and used to calculate wave speeds using Eqs. (1) and (2). The joint probability distribution, and cumulative distribution for composite stiffness, C_{66} and angle of fiber orientation, θ is shown in Fig. 5.

Wave speeds were calculated by sampling from this joint distribution; these results are shown by scatter plots in 6. Fig. 6a, b, and c show the solution of the transverse wave equation (Eq. (1)).

Quasi-longitudinal and quasi-transverse waves are also considered (Eq. (2)). The two roots of Eq. (2) correspond to waves that are neither purely longitudinal (with displacements in the same direction as the propagating wave) nor purely transverse. They have quasi-longitudinal and quasi-transverse components. Fig. 6d, e, and f show solutions for the negative real roots of Eq. (2) (quasi-transverse). Fig. 6g, h and i show solutions for the positive real roots of Eq. (2) (quasi-longitudinal). Quasi-longitudinal waves have velocities approximately an order of magnitude higher than transverse and quasi-transverse waves [1].

For each type of wave (transverse, quasi-transverse and quasi-longitudinal) represented by the three columns of Fig. 6, a three dimensional scatter plot is given (Fig. 6a, d and g). To visualize the three dimensional scatter plot from different directions, projections are given showing only θ varying (Fig. 6b, e and h). Projections are also given showing only C_{66} varying (Fig. 6c, f, i).

The variation of θ centered around $\theta = 0$ shows the arch- and inverted arch-type variation characteristic of the analytic functions plotted in Fig. 2. Wave speeds for the transverse and quasi-longitudinal waves decrease with increasing orientation angles. Waves speeds for the quasi-transverse wave component increase with increasing angle.

The scatter shown in the projections in Fig. 6b, e and h is due to the variation in material property. The wave speeds show greatest scatter near the region where $\theta = 0$. Over the full range of θ shown, the range of the transverse wave speeds is almost 80% of the minimum speed; the range of the quasi-transverse are roughly 12% of their minimum; the range of the quasi-longitudinal are almost 14% of their minimum value.

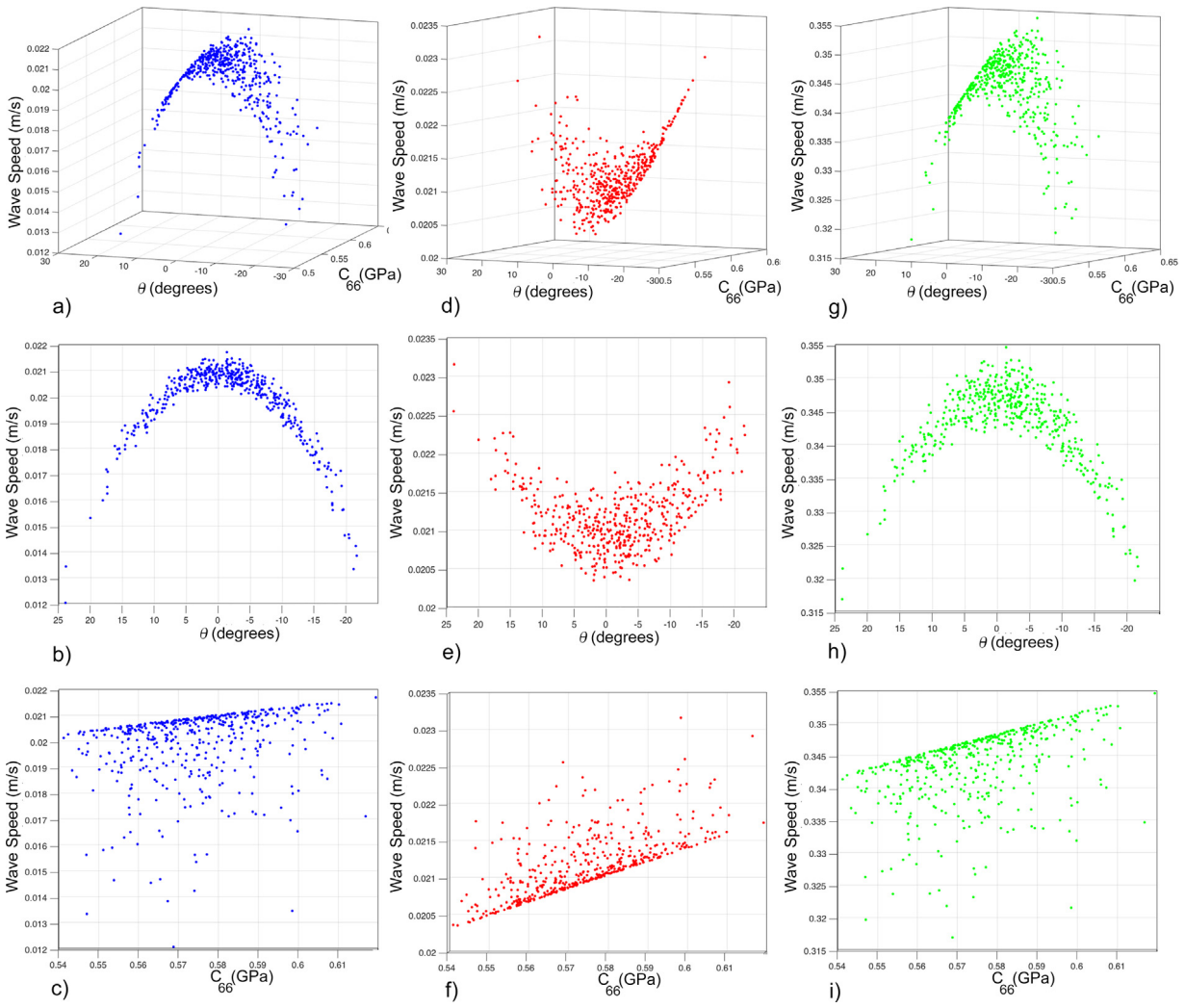

Fig. 6. Scatter Plots of waves speeds associated with simulated parameters C_{66}, θ. In the first column, figs. a, b and c show results for transverse waves (Eq. (1)). In the second column, figs. d, e, and f show results for quasi-transverse waves (negative real root Eq. (2)). In the third column, figs. g, h, and i show results for quasi-longitudinal waves (positive real root Eq. (2)). The top row shows a 3D view of waves speeds as a function of stiffness and angle orientation (figs. a, d, g). The center row looks through the 3D scatter plot from the perspective of varying (θ figs. b, e, h). The bottom row looks through the 3D scatter plot from the perspective of varying C_{66} (figs. c, f, i).

Where only the variation in material property is considered (projections in Fig. 6c, f, g), wave speed increases with increasing values of C_{66}. The majority of the data points are approaching this line; however, significant outlying data points are scattered far from this line, without preferential location with respect to the value of C_{66}.

The effect of angular mis-alignment, based on the assumed distribution of θ used in the analysis, begins at approximately $\pm 3°$. Near $\theta = 0°$, ($\pm 10°$), increasing stiffnesses affect wave speeds more than increasing angle. At large angles, both large and small stiffness can produce similar, lower, waves speeds.

6. Summary and conclusions

The statistics described by a population of SVE was used to characterize variability of composite properties in a transversely isotropic fiber reinforced composite. The angle of wave propagation relative to fiber orientation was considered a Gaussian random variable. Based on this characterization, a probabilistic simulation of wave speeds in a high a contrast random composite was performed using a joint probability distribution function to sample a material stiffness and fiber angle of orientation.

It was found that the use of probability distributions based on SVE material properties is an effective way to introduce variability into a simulation of material behavior under uncertain load (in this case, wave speed under an uncertain angle of wave orientation). In a general sense, using SVE material property distributions allows for a comparative analysis of which uncertain parameter has more bearing on the results of a mechanical analysis. Under the conditions presented here, it has been shown that wave orientation angle has relatively more significance than the variation in material property in a wave speed analysis.

The variation in material properties has been captured based on the morphology of the material microstructure. The relationship between SVE size δ and the variability introduced in the analysis is well understood through the hierarchy of bounds on material effective behavior. In an application where a conservative approach calls for over-estimation of the material stiffness, the current approach can be used to bound the effective property from above. Where a conservative approach calls for under-estimation of material stiffness, an SVE analysis based on statically uniform boundary conditions could be used. In this way, conservative numerical simulations can be developed to capture uncertainty in the response of a population of nominally identical samples with randomly varying microstructure.

In future work it would be useful to consider the effect of the assumed distributions of θ. This could affect the angle where the effects start to take place, ($\leq \pm 3°$) as well as the relative impact of the variable

stiffnesses. An investigation of the different partition sizes, potentially weakening the assumption of transverse isotropy, but increasing the bounds on stiffnesses would also be interesting. Finally, the effect of contrast ratio, relatively high in the presented work, should be considered.

References

[1] G.D. Dean, F.J. Lockett, Determination of the mechanical properties of fiber composites by ultrasonic techniques, in: Analysis of the Test Methods for High Modulus Fibers and Composites, ASTM International, 1973.

[2] R.D. Kriz, W.W. Stinchcomb, Elastic moduli of transversely isotropic graphite fibers and their composites, Exp. Mech. 19 (2) (1979) 41–49.

[3] J. Guilleminot, C. Soize, D. Kondo, Mesoscale probabilistic models for the elasticity tensor of fiber reinforced composites: experimental identification and numerical aspects, Mech. Mater. 41 (12) (2009) 1309–1322.

[4] L. Thomsen, Weak elastic anisotropy, Geophysics 51 (10) (1986) 1954–1966.

[5] P.F. Daley, F. Hron, Reflection and transmission coefficients for transversely isotropic media, Bull. Seismol. Soc. Am. 67 (3) (1977) 661–675.

[6] J.M. Carcione, Wave Fields in Real Media: Wave Propagation in Anisotropic, Anelastic, Porous and Electromagnetic Media, Vol. 38, Elsevier, 2007.

[7] M.J.P. Musgrave, Deviation of ray from wave normal for elastic waves in principal planes of crystal symmetry, J. Mech. Phys. Solids 18 (3) (1970) 207–211.

[8] G.E. Backus, Long-wave elastic anisotropy produced by horizontal layering, J. Geophys. Res. 67 (11) (1962) 4427–4440.

[9] I.M. Gitman, H. Askes, L.J. Sluys, Representative volume: Existence and size determination, Eng. Fract. Mech. 74 (16) (2007) 2518–2534.

[10] M. Ostoja-Starzewski, Material spatial randomness: From statistical to representative volume element, Probab. Eng. Mech. 21 (2) (2006) 112–132.

[11] S. Hazanov, C. Huet, Order relationships for boundary conditions effect in heterogeneous bodies smaller than the representative volume, J. Mech. Phys. Solids 42 (12) (1994) 1995–2011.

[12] C. Huet, Application of variational concepts to size effects in elastic heterogeneous bodies, J. Mech. Phys. Solids 38 (6) (1990) 813–841.

[13] Tarek J. Zohdi, Peter Wriggers, Introduction to Computational Micromechanics, in: Lecture Notes in Applied and Computational Mechanics, vol. 20, 2005.

[14] K.A. Acton, S.C. Baxter, Characterization of random composite properties based on statistical volume element partitioning, J. Eng. Mech. 144 (2) (2017) 04017168.

[15] M. Salmi, F. Auslender, M. Bornert, M. Fogli, Apparent and effective mechanical properties of linear matrix-inclusion random composites: Improved bounds for the effective behavior, Int. J. Solids Struct. 49 (10) (2012) 1195–1211.

[16] L.L. Graham, S.C. Baxter, Simulation of local material properties based on moving-window gmc, Probab. Eng. Mech. 16 (4) (2001) 295–305.

[17] S.C. Baxter, L.L. Graham, Characterization of random composites using moving-window technique, J. Eng. Mech. 126 (4) (2000) 389–397.

[18] E.J. Barbero, Introduction to Composite Materials Design, CRC Press, 2017.

[19] J. Guilleminot, C. Soize, Stochastic model and generator for random fields with symmetry properties: Application to the mesoscopic modeling of elastic random media, Multiscale Model. Simul. 11 (2013) 840–870.

[20] A.I. Beltzer, T. Sato, Probability distribution of wave velocity in heterogeneous media due to random phase configuration, Wave Motion 38 (3) (2003) 221–227.

[21] C.E. Shannon, A mathematical theory of communication, Bell Syst. Tech. J. 27 (1948) 379–423.

[22] C. Soize, Tensor-valued random fields for meso-scale stochastic model of anisotropic elastic microstructure and probabilistic analysis of representative volume element size, Probab. Eng. Mech. 23 (2008) 307–323.

[23] K. Sobczyk, Reconstruction of random material microstructures: patterns of maximum entropy, Probab. Eng. Mech. 18 (4) (2003) 279–287.

[24] R. Bourn, B.S. Fralick, S.C. Baxter, Distributions of elastic moduli in mechanically percolating composites, Probab. Eng. Mech. 34 (2013) 67–72.

[25] E. Jaynes, Probability Theory: The Logic of Sciences, Cambridge University Press, 2003.

[26] C. Walck, Hand-book on statistical distributions for experimentalists, No. SUF-PFY/96?01, 1996.